Upcycling stale bread into (meso)porous materials: Xerogels and aerogels

Wanxiang Guo, Tatiana Budtova, Mario M Martinez

Food Hydrocolloids 160 (2025) 110807

Contents lists available at ScienceDirect

Food Hydrocolloids

journal homepage: www.elsevier.com/locate/foodhyd

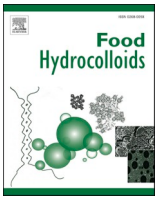

Upcycling stale bread into (meso)porous materials: Xerogels and aerogels

Wanxiang Guo [a], Tatiana Budtova [b,**], Mario M. Martinez [a,c,*]

[a] Center for Innovative Food (CiFOOD), Department of Food Science, Aarhus University, Agro Food Park 48, Aarhus, N 8200, Denmark
[b] Mines Paris, PSL University, Center for Materials Forming (CEMEF), UMR CNRS 7635, CS 10207, 06904, Sophia Antipolis, France
[c] InnograinLab, Food Technology Division, Department of Agricultural Engineering, University of Valladolid, Spain

ARTICLE INFO

Keywords:
Starch
Absorbent pad
Packaging
Food waste
Bio-based materials

ABSTRACT

This work explores the upcycling of stale bread into bio-based, low-density porous materials with partial mesoporosity, produced through gelatinization and drying, using either supercritical CO_2 (aerogels) or low-vacuum conditions (xerogels). Cryogels were also fabricated via freeze-drying for comparison purposes. Stale bread particles (Bread) were subjected to proteolytic gluten depletion (Gluten-Depleted Bread, GDB) or particle size reduction (Finely milled Bread, FB) to investigate the effect of protein removal or particle size on porous materials' properties. Porous materials made from wheat starch (WS) and wheat flour (Flour) were also examined for comparison. The solvent exchange induced volume shrinkage (SE-VS), which accounted for over 87% of the total shrinkage, ranged from 62% in GDB to 78% in WS. Bread-based porous materials presented comparable specific surface area (~40 m^2/g) and water absorption capacity (~400%) to WS materials, but outperformed in resistance to volume shrinkage, resulting in lower density. FB porous materials possessed a higher specific surface area than Bread materials, indicating the benefits of particle size reduction. Furthermore, gluten depletion resulted in GDB-aerogels with the highest specific surface area (~80 m^2/g), highlighting the benefits of gluten depletion. However, WS materials exhibited significantly greater maximum compressive stress (>2.0 MPa) and compressive modulus (>6 MPa) than stale bread-based porous materials. Importantly, the porous properties of xerogels and aerogels were similar (differences < 10%), indicating the feasibility of using low vacuum drying to produce new porous materials with partial mesoporosity (surface area 60–80 m^2/g) from stale bread at a lower cost.

1. Introduction

Bakery waste ranks at the top of the food waste categories in terms of volume (up to 30% of waste by mass) (Brancoli et al., 2017) and environmental footprint (Brancoli et al., 2019, 2020; Eriksson et al., 2015). Among the food waste management options in the supermarket, stale bread displays the greatest influence on carbon footprint (Eriksson et al., 2015). Furthermore, bread waste is inducing notable economic and bioresource losses (Brancoli et al., 2020; Dymchenko et al., 2023; Kumar et al., 2022). Fortunately, the distribution scheme of bread makes it an ideal product for large-scale redistribution and recovery strategies (Gómez & Martinez, 2023), which may not always be feasible for other food waste fractions. This is because bread waste is mostly generated at the retailer-supplier interface due to consumers preferences for fresh bread and the rapid physical spoilage due to staling (Brancoli et al., 2019; Dymchenko et al., 2023; Franco et al., 2024; Gómez & Martinez, 2023; Narisetty et al., 2021). Thus, bread waste represents an abundant source of biopolymers featured by uniform composition and low microbial risk (Gómez & Martinez, 2023).

The redistribution of bread waste into animal feed and human foods has gained attention, although the absence of specific regulations for the use of novel by-products could challenge most redistribution pathways (Gómez & Martinez, 2023). Bread waste has been considered as feedstock for the fermentative production of chemical building blocks (Kumar et al., 2022; Narisetty et al., 2021), although the need for liquefaction and acidic/enzymatic saccharification to be used as fermentation feedstock compromises production costs (Kumar et al., 2022). In any case, macromolecules in bread present high molecular weight, a wide range of chemical moieties and inter- and intramolecular interactions, inviting for research to directly repurpose bread waste into a matter of higher value and under less resource-demanding processes than fermentable sugars: as building blocks of future biomaterials (e.g.,

* Corresponding author. Centre for Innovative Food (CiFOOD), Department of Food Science, Aarhus University, Agro Food Park 48, Aarhus, N 8200, Denmark.
** Corresponding author.
E-mail addresses: tatiana.budtova@minesparis.psl.eu (T. Budtova), mm@food.au.dk, mmartinez@uva.es (M.M. Martinez).

https://doi.org/10.1016/j.foodhyd.2024.110807
Received 26 August 2024; Received in revised form 20 October 2024; Accepted 31 October 2024
Available online 1 November 2024

flexible films or materials with controlled porosity).

White bread is mostly comprised of refined wheat flour (i.e., starchy endosperm), consisting of ~80% (dry basis d.b.) starch, 8–12% (d.b.) proteins, and 7% (d.b.) plant cell walls (Gruppen et al., 1989; Guo et al., 2024). It is noted that although milled bread particles are compositionally similar to wheat endosperm flour, the bread-making process results in marked differences in the molecular and supramolecular structure of starch, cell wall polysaccharides and gluten proteins. Guo et al. (2024) reported that these changes mostly consisted of starch gelatinization, chain scission of starch and arabinoxylans (significantly decreasing their molar mass), the insolubilization of cell wall material, the development of a stranded and entangled gluten network, and the formation of dispersed gluten microparticles. More specifically, these authors observed a reduction in the molecular weight (M_w) of amylopectin (51.8×10^6 vs 425.1×10^6 g/mol) and water extractable arabinoxylans WEAX (1.79×10^5 vs 7.63×10^5 g/mol), and a decrease in amylose length (245 vs 748 glucose units) after bread-making. Furthermore, storage after baking leads to staling, characterized by starch retrogradation, moisture redistribution among bread biopolymers, and moisture loss (Franco et al., 2024), allowing stale bread to be efficiently converted into particles through conventional milling (Gómez & Martinez, 2023; Guo et al., 2024). Despite these transformations, the simple combination of bread waste with plasticizer resulted in visually intact, relatively transparent, and flexible self-standing films (Guo et al., 2024). In fact, bread films possessed good light-blocking performance (< 30% transmittance) and 2,2-diphenyl-1--picrylhydrazyl (DPPH)-radical scavenging capacity and even presented lower hygroscopicity and greater elongation at break than films made from wheat flour, setting a precedent for the large-scale upcycling of bread waste into valuable biomaterials.

Bio-based porous materials with low density and high specific surface area, as well as biodegradable and often biocompatible, are gaining interest to be used as absorbent agents, loose-fill cushioning materials, or even delivery systems or thermal insulators, which renders multiple opportunities in medical, food and packaging applications (Druel et al., 2017; Zheng et al., 2020; Zhu, 2019; Zou & Budtova, 2021a). The fabrication of bio-based porous materials includes the dissolution of biopolymers (typically polysaccharides), gelation (sometimes this step can be omitted), solvent exchange (if needed), and drying. Depending on the drying approaches and the resulting properties, porous materials can be classified as cryogels, aerogels and xerogels. Cryogels are prepared via freeze-drying, typically resulting in a fragile porous structure with low density and high porosity and very large macropores due to the growth of ice crystals (Zou & Budtova, 2021b). Aerogels are of low density and high specific surface area; they are usually formed by removing the liquid component from the gel through drying in supercritical conditions, usually with CO_2 ($scCO_2$), to avoid the liquid-gas phase boundary and preventing the collapse of the porous structure. For this reason, aerogels are lightweight nanostructured mesoporous materials, becoming excellent thermal insulators (Druel et al., 2017; Ma et al., 2022; Zou & Budtova, 2021a). Xerogels are formed by removing the liquid component from the gel through conventional drying methods, such as evaporation. This process typically leads to shrinkage and collapse of the porous structure, usually resulting in materials with low porosity and high density. Specially, the fabrication of aerogels requires a high-pressure technology, which leads to a high cost, and potentially restrains their applications. A recent study reported that starch xerogels made by low-vacuum evaporative drying could exhibit similar properties than aerogels (Zou & Budtova, 2023), showing a new pathway in making aerogel-like polysaccharide materials without drying in supercritical conditions.

The low price, renewability, and abundance of starch have positioned it at the center stage for the fabrication of bio-based porous materials (Ahmadzadeh & Ubeyitogullari, 2023; Alavi & Ciftci, 2022; Ubeyitogullari & Ciftci, 2016; Ubeyitogullari et al., 2018, 2019; Zou & Budtova, 2023). For example, in the early 1990s, biodegradable starch-based loose-fill packaging materials were developed as a more environmentally friendly alternative to polystyrene (Campanella, 2014). Whether cryogel, xerogel or aerogel, starch gelatinization represents, in most cases, the first fundamental step in the fabrication of starchy porous materials. Since stale bread mostly consists of starch, that in fact underwent gelatinization, we hypothesized that stale bread could be directly upcycled into porous materials such as cryogels, xerogels and aerogels, some of them with partial mesoporisity. At this point, a mechanistic investigation was, however, warrantied, since stale bread consists of multiple and interacting polymeric components that underwent shear scission, molar mass decrease and/or aggregation during the bread-making process (Guo et al., 2024).

This work aims to explore, for the first time, the direct upcycling of stale white bread into bio-based porous materials (cryogels, xerogels and aerogels) of tuneable porosity, surface area and mechanical performance. Xerogels and aerogels were fabricated via low-vacuum and $scCO_2$ drying, respectively, using stale bread, water and ethanol as the only components. Cryogels (made by freeze-drying) were also fabricated for comparison purposes, serving as macroporous benchmarks. In terms of raw materials, porous materials from gluten-depleted stale bread (via enzymatic proteolysis), as well as finely milled stale bread, were also included in this study, to investigate the effect of protein and particle size on materials' properties, respectively. Porous materials made from commercial wheat starch or wheat flour were also included as controls.

2. Materials and methods

2.1. Materials, chemical supplies, and bread-making

White wheat flour (Flour, falling number 340 s, alveogram W 180×10^{-4} J) was supplied by Molinos del Duero-Carbajo Hermanos S.A. (Zamora, Spain). Breads were made at industrial scale and kindly donated by La Tahona de Sahagun S.L. (Spain). Breads presented 1.8% salt (wheat flour basis, f.b.), 2.0% (f.b.) fresh yeast, and 0.8% (f.b.) Pulso Ecopan enzymatic improver (Lesaffre Iberica, Spain). Breads were stored for 15 days in room conditions (room temperature and without controlling relative humidity) and then milled into bread particles (Bread) using an ultra-centrifugal mill (ZM 200, Retsch Düsseldorf, Germany) equipped with a 500 μm mesh screen. The selected storage conditions were based on several factors. Firstly, breads with shorter shelf lives, like baguettes, are often kept at room temperature in distribution centers. Secondly, while these breads are usually eaten on the same day they are baked, a 15-day storage period better aligns with the typical collection timeframe for bread waste. Lastly, a 15-day storage period ensured significant staling without visible microbial spoilage, replicating the state in which stale bread is commonly found. To study the influence of the particle size on the porous material properties, stale bread particles were further ground into smaller particle size with a coffee grinder (Bodum, Denmark) and sieved with a 45 μm mesh screen. This finely milled bread particles are denoted as FB. Commercial wheat starch (WS) was supplied by Roquette (Spain). The procedures for sample preparation of starchy materials are summarized in Fig. 1.

Ethanol (> 99%) was purchased from Fisher Chemical. Protease from *Streptomyces griseus* (P5147, Type XIV, ≥ 3.5 units/mg solid) was purchased from Sigma-Aldrich (St Louis, MO, US). Total starch HK assay kit was purchased from Megazyme International Ltd. (Wicklow, Ireland). Dimethyl sulfoxide (DMSO) was purchased from VWR (Avantor, Inc., US). Other chemicals were all purchased from Sigma-Aldrich (St Louis, MO, US).

2.2. Gluten depletion in stale bread particles

To study the influence of gluten on the properties of porous materials, stale bread particles were subjected to protein hydrolysis as follows. Bread particles were dispersed in protease solution (pH 7.5, 100 mM Na_2HPO_4/NaH_2PO_4) at a ratio of 1000 g of flour per gram of

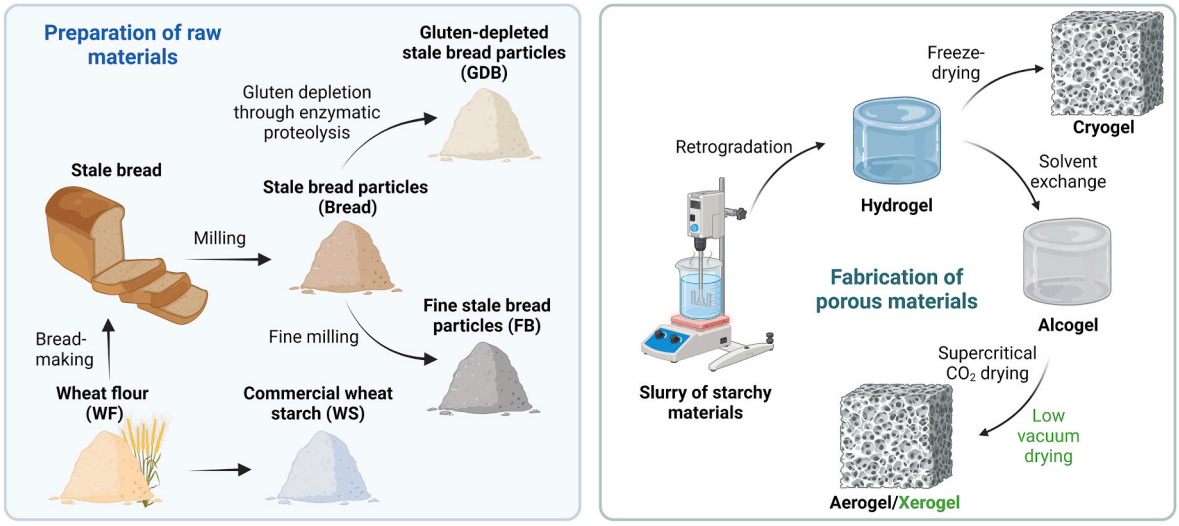

Fig. 1. Preparation of stale bread powders (left) and porous materials (right).

Streptomyces griseus protease and incubated at 37 °C for 4 h, followed by centrifugation at 4000 rpm for 30 min. Pellets were then dispersed in 0.45% w/w $NaHSO_3$ and incubated at 37 °C for 30 min, followed by the centrifugation conditions mentioned above. Then, samples were frozen at −80 °C overnight followed by freeze-drying at −85 °C below 1 mbar for 3 days (Delta 2–24 LSCplus, Christ, Germany). Gluten-depleted bread particles are denoted as GDB.

2.3. Composition and starch fine structure and hydrodynamics in DMSO

Starch and protein (N × 5.71) content in the commercial WS, Flour and various bread particles (Bread, FB and GDB) was determined according to approved AACC methods 76-13 and 46-30 (AACC, 2010), respectively. All determinations were conducted in duplicate.

Molecular weight and chain length distribution of amylose and amylopectin were analysed at least in duplicate using a high-performance size-exclusion chromatography system (HPSEC, Agilent 1260 infinity II, CA, US) equipped with a refractive index detector (RID, Shodex RI-501, NY, US) and multi-angle light scattering detector (MALS, Wyatt Technology Corporation, CA, US). Using 0.5 % w/w DMSO/LiBr, branched starch was eluted at 80 °C with a flow rate of 0.3 mL/min, while debranched starch was run at a flow rate of 0.6 mL/min at the same temperature. Amylose ratio, expressed as the mass proportion of amylose relative to the total starch content, was determined from the SEC molecular weight distribution of debranched starch as the ratio of the area under the curve (AUC) of amylose branches to the AUC of overall amylopectin and amylose branches. The details of starch extraction, purification, and measurement conditions can be found in the previous work (Guo et al., 2024). A set of pullulan standards (P-82, Shodex, Germany), maltose, and maltohexaose were applied for calibration.

2.4. Fabrication of cryogels, xerogels and aerogels

The procedures for the fabrication of porous materials are shown in Fig. 1. These procedures mainly involve the preparation of hydrogels, followed by either freeze-drying to obtain cryogels or solvent exchange and subsequent supercritical CO_2 drying or low vacuum drying to produce aerogels or xerogels, respectively.

2.4.1. Hydrogel formation and fabrication of cryogels

Raw materials (WS, Flour, Bread, FB or GDB) were individually dispersed in distilled water at a concentration of 10% w/w. The sample dispersion was then subjected to hydrothermal processing at 95 °C for 3 h with mechanical stirring at 300 rpm using an overhead mixer (Heidolph, Germany) in order to ensure starch gelatinization. The dispersion was then poured into cylindrical plastic moulds and cooled at room temperature. Retrogradation was then implemented at 4 °C for 3 days to obtain self-standing hydrogels.

Cryogels, as an example of highly macroporous materials, were prepared from the hydrogels by lyophilization. Hydrogels were frozen by fully immersing the plastic moulds in liquid nitrogen and then freeze-dried at −85 °C at 10 mTorr using a Cosmos-80 lyophilizer (Cryotec, France) for 3 days.

2.4.2. Solvent exchange and fabrication of xerogels and aerogels

In this study, ethanol was applied to eliminate the water from hydrogels, thereby obtaining the so-called alcogels (Fig. 1). Ethanol was selected due to its lower surface tension compared to water for further evaporative drying and due to its miscibility with water and CO_2 for further drying with $scCO_2$ (Zou & Budtova, 2023). Sequential solvent exchange was performed with 50 %, 75 % and 100 % (v/v) ethanol/-water solution. Each ethanol concentration was maintained for two days with daily solvent refreshing. A sequential solvent exchange was chosen to avoid the rapid and uneven shrinkage associated with the direct immersion of hydrogel in pure ethanol. Gradual replacement of water in hydrogels with ethanol at different concentrations allows for a more controlled dehydration process, reducing the likelihood of structural damage leading to the micro-cracking observed in our preliminary experiments. This stepwise approach ensured uniform shrinkage of the hydrogel and preserved the integrity of its porous structure, which is crucial for maintaining the functionality of the final material.

Xerogels were obtained from alcogels by drying at 50 °C overnight under low vacuum (~3 kPa) using a VT5042 vacuum oven (Heraeus, Germany). Aerogels were obtained using a supercritical CO_2 extraction system. Details of the drying conditions and procedures were given elsewhere (Zou & Budtova, 2021b).

2.5. Characterization of porous materials

2.5.1. Morphology

Scanning electron microscope (SEM) was used to analyze the microstructure of materials. Samples were coated with platinum and analysed using a Nova SEM 600 (FEI, USA) with an accelerating voltage of 5 kV.

Confocal laser scanning microscopy was adapted to determine the spatial distribution of proteins and starch. Samples were hydrated with distilled water for better staining. Proteins were stained by both

Rhodamine B (1 mg/ml) and fluorescein isothiocyanate (FITC, 1 mg/ml), whereas FITC was used to stain starch as well, offering a differentiating signal to represent the distribution of protein and starch. The excitation wavelengths of Rhodamine B and FITC were set at 561 nm and 488 nm, respectively. The emission spectra were detected at 571–625 nm (Rhodamine B) and 505–551 nm (FITC). The images (884 × 884 μm) were captured by Nikon AX laser scanning microscope (Nikon Corporation, Japan) and processed by NIS elements (Nikon Corporation, Japan). By converging the Rhodamine B-stained and FITC-stained images, the presence of starch was represented by green pixels, while the proteins were indicated by the red or orange pixels.

2.5.2. X-ray diffraction analysis

Wide angle X-ray diffraction (XRD) analysis was performed using a diffractometer "XPERT-PRO" (PANalytical) equipped with Cu Kα radiation with a wavelength of 1.5406 Å. The X-ray generator was operated at 40 kV. Sample was ground into power and scanned from 5° to 40° with a step of 0.02°.

2.5.3. Volume shrinkage

The volume shrinkage of samples in the shape of disks, caused by solvent exchange (SE-VS) and after the whole fabrication process (F-VS), was calculated equations (1) and (2). The volume shrinkage from the drying step was calculated as the difference between SE-VS and F-VS. The diameter and the height of the sample was measured in triplicates using a digital caliper (ABS, Mitutoyo, Japan).

$$\textit{Volume shrinkage due to solvent exchange} = \frac{V_0 - V_1}{V_0} \times 100\% \quad (1)$$

$$\textit{Fabrication Volume shrinkage} = \frac{V_0 - V_2}{V_0} \times 100\% \quad (2)$$

where V_0 and V_1 represent the volume before and after solvent exchange, respectively; V_2 represents the volume after whole fabrication.

2.5.4. Bulk density, porosity and specific surface area

Bulk density (ρ_b) of porous materials was calculated from sample mass, measured using a high-precision balance, and volume, measured using a density analyzer (Geopyc 1360, Micromeritics, USA). The diameter of the test chamber was 19.1 mm and DryFlo was used as the test medium. The consolidation force was set as 25 N. The measurements were repeated five times.

The porosity of the sample was calculated according to equation (3):

$$\textit{Porosity} = \frac{\rho_b - \rho_s}{\rho_b} \times 100\% \quad (3)$$

where ρ_s represents starch skeletal density, 1.5 g/cm^3 (Dengate et al., 1978).

Brunauer-Emmett-Teller specific surface area (S_{BET}) was determined with low-temperature nitrogen absorption method using a surface area and porosity analyser (ASAP 2020, Micromeritics, USA). Degassing was performed prior to the analysis at 70 °C overnight.

2.5.5. Water absorption capacity

The water absorption capacity (WAC) was conducted to test the potential porous materials as absorbent pad according to Wang et al. (2024). Sample was dried at 60 °C for 24 h to remove the moisture, cooling down and then immersed in distilled water for another 24 h at room temperature. Water droplets on the sample surface was removed by laboratory tissue paper and the weight of sample before and after soaking was measured. The water absorption capacity was calculated according to equation (4):

$$WAC = \frac{m_1 - m_0}{m_0} \times 100\% \quad (4)$$

where m_0 and m_1 represent the weight of sample before and after soaking, respectively.

2.5.6. Mechanical properties

Uniaxial compression test was applied using a Texture Analyzer (Mecmesin, FTC, USA) with a load cell of 1 kN at a compression rate of 1 mm/min (Buchtova et al., 2019). Samples were polished with P240 sandpaper before compression to obtain a cylinder with flat and parallel upper and lower planes. The compression test was repeated five times. Stress-strain dependences were recorded and maximum compressive stress, compressive modulus, and strain at failure were determined.

2.6. Statistical analysis

Statistical difference among groups was analysed by one-way analysis of variance (ANOVA). Post-hoc analysis was conducted using TukeyHSD to describe means with 95% confidence intervals. Data analysis was performed by OriginPro (2023b, OriginLab, US).

3. Results and discussion

3.1. Composition, starch fine structure, starch hydrodynamics in DMSO and morphology of raw materials

Stale bread particles (Bread) mostly consisted of starch (77.8% dry basis, d.b.) with a moderate amount of protein (10.6% d.b.), as shown in Table 1. Compositionally, Bread and its parent wheat flour (Flour) presented similar starch and protein content, whereas Gluten-depleted bread (GDB) presented significantly lower protein and higher starch content, respectively, confirming a successful gluten depletion. It is noted that a complete gluten removal was not attained since some proteins can be highly interacting with the matrix components and, hence, not accessible for enzymatic proteolysis (Guo et al., 2024). Commercial wheat starch (WS), which was used as a control in this study, possessed the greatest starch content (95.1% d.b.) and the lowest protein content (0.2% d.b.), being similar to GDB.

The weight average molecular weight, amylose ratio and chain length distribution for the starch present in the samples used in the work are presented in Table 1 and Fig. 2A. Finely milled bread (FB) was not analysed since it is not expected to differ from its coarsely milled counterpart (Bread), as milling has been shown to affect only those starch molecules that are in the periphery of cereal particles, which represent a minority and hence does not affect the chain length profiles (Roman et al., 2017). Results of amylose and amylopectin chain length distribution and amylopectin molecular weight M_w showed no differences between Bread and GDB, indicating no effect of protease

Table 1
Composition and starch features of wheat starch (WS), Flour, Bread and gluten-depleted bread (GDB).

	Protein (% d.b.)	Starch (% d.b.)	Amylopectin	Amylose	
			M_w (× 10^6 g/mol)	DP (Glucose units)	Ratio (%)
WS	0.2 ± 0.1	95.1 ± 3.7	266.9 ± 0.6^b	1093 ± 13^a	26.2 ± 0.2^b
Flour	10.6 ± 0.1	79.8 ± 1.0	500.7 ± 1.1^a	748 ± 57^b	27.9 ± 1.8^b
Bread	10.6 ± 0.1	77.8 ± 1.0	71.1 ± 3.7^c	245 ± 13^c	33.4 ± 1.7^a
GDB	1.7 ± 0.1	94.0 ± 0.1	70.1 ± 0.2^c	328 ± 3^c	33.4 ± 0.2^a

Letters within same column indicate statistically significant difference ($p < 0.05$). The average length of amylose chains is presented as degree of polymerization (DP) at the peak maximum attributed to amylose. The amylose ratio refers to the mass proportion of amylose relative to the total starch content, which includes both amylose and amylopectin.

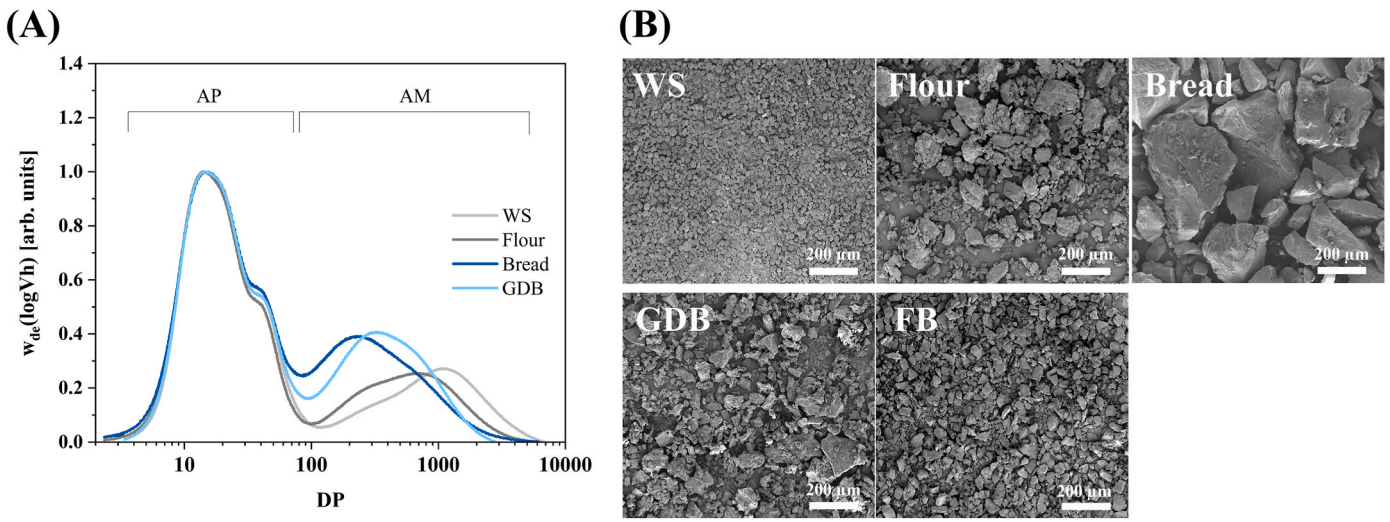

Fig. 2. Size exclusion chromatogram of debranched starch samples (A), showing chain length distribution of amylopectin and amylose, and SEM images (B) of wheat starch (WS), wheat flour (Flour), bread particles (Bread), gluten-depleted bread particles (GDB) and finely milled bread particles (FB).

treatment on starch structural features. Nevertheless, WS and Flour presented greater amylopectin M_w (> 266.9 × 10^6 g/mol) and average amylose length (> 748 glucose units, GU) than Bread and GDB particles, the latter with M_w < 71.1 × 10^6 g/mol and average amylose length < 328 GU. These results agree with the effects of bread-making on starch molecular weight shown by Guo et al. (2024), who hypothesized chain scission due to shear force through the bread-making and high temperature during baking as the mechanisms responsible for amylose and amylopectin molecular weight loss. Amylose ratio was similar in Bread and GDB, and slightly higher in WS and Flour, which could be explained by co-elution of degraded (size-reduced) amylopectin with amylose, which would consequently increase amylose ratio as measured by SEC. WS possessed different starch chain length distribution than Flour, which can be ascribed to the different wheat variety and the fact that WS came from a different manufacturer. SEM images of all materials are presented in Fig. 2B, showing the lower particle size of finely milled bread compared to stale bread particles.

3.2. *Visual appearance and morphology of cryogels, xerogels, and aerogels*

First, we considered the appearance, handling and morphology of all samples in order to select the ones for a further deeper investigation. Cryogels are examples of porous materials fabricated using the commonly available freeze-drying approach. All cryogels showed cracking after freeze-drying and displayed a visible cone attributed to the anisotropic growth of ice crystals (Fig. S1). The absence or deliberate depletion of gluten (i.e. WS or GDB, respectively) resulted in cryogels with smaller pores and pore walls similar to shattered pieces, in particular, in the case of GDB (Fig. S2). On the contrary, cryogels made from Flour and Bread displayed a hierarchical morphology with large pores and pore walls having small pores. It was demonstrated that amylose ratio strongly influences the morphology of aerogels made via drying with supercritical CO_2 (Druel et al., 2017; Zou & Budtova, 2021b). As far as amylose ratio is practically the same in all initial materials, these results highlight the role of protein in cryogel morphology. Presumably, the highly polymerized gluten network, which is water insoluble, negatively impacted the formation of a uniform and interconnected starch network, possibly due to the spatial hindrance between starch chains or starch-rich areas, in agreement with a previous study (Falua et al., 2023). The result obtained suggests that starch composition plays an important role in cryogel morphology, as shown in other works (Barros et al., 2024; Falua et al., 2023). All cryogels present large macropores ranging from few microns to several tens and even hundreds of microns.

The images of starch aerogel and xerogel are presented in Fig. 3. All prepared samples were integral and uniform with no cracking and pores much smaller than in cryogels (Fig. 4). Remarkably, the pore diameter of the xerogels and aerogels ranged from tens to hundreds of nanometers, exhibiting a certain level of mesoporosity. Altogether, images indicated that $scCO_2$ and low vacuum drying are more suitable to fabricate intact porous materials from our starchy ingredients than freeze-drying. It is important to note that the morphology of aerogels and xerogels is very similar showing that low-vacuum drying can replace high-pressure technology, as also demonstrated for potato starch (Zou & Budtova, 2023). Both xerogels and aerogels displayed a visible three-dimensional network as reported in other studies (Ubeyitogullari & Ciftci, 2016; Zou & Budtova, 2021b). The microstructure of xerogels and aerogels made from stale bread materials (Bread, FB, GDB) was comparable to that of native WS, providing preliminary evidence about the feasibility of upcycling bread waste to fabricate finely porous materials. However, xerogels and aerogels still displayed some non-porous regions in bulk, which was likely attributed to poorly dissolved starch (Fig. 4). A higher

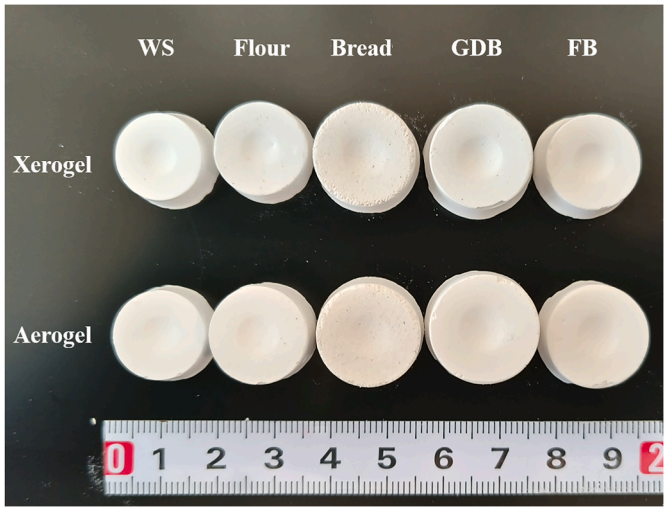

Fig. 3. Morphology of xerogels and aerogels made from wheat starch (WS), wheat flour (Flour), bread particles (Bread), gluten-depleted bread particles (GDB) and finely milled bread particles (FB).

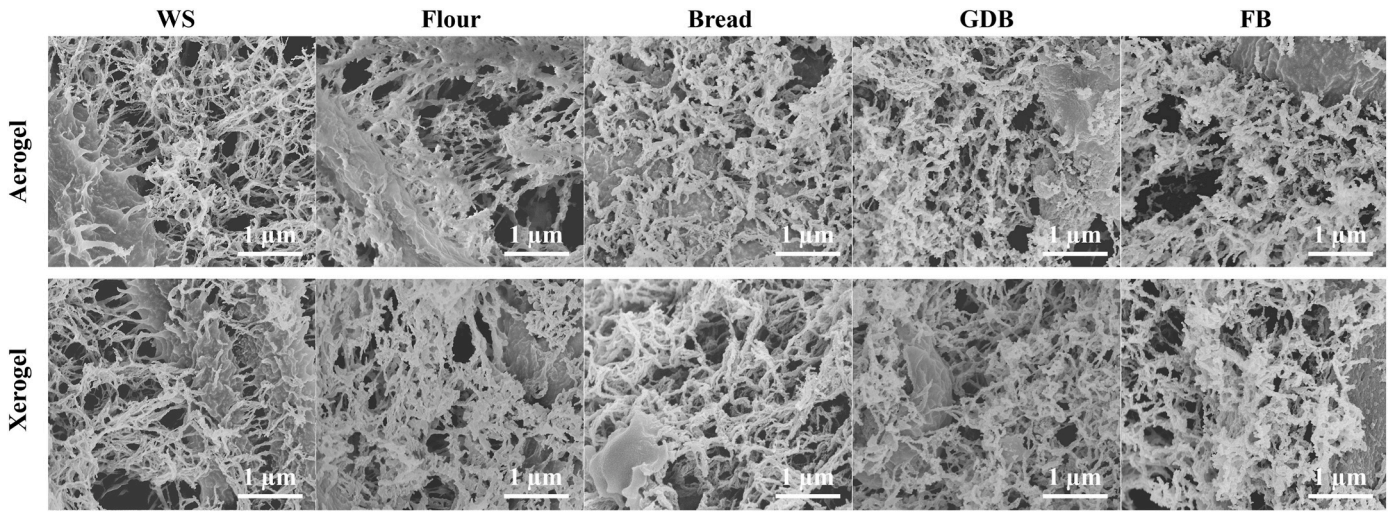

Fig. 4. SEM images of xerogels and aerogels made from wheat starch (WS), wheat flour (Flour), bread particles (Bread), gluten-depleted bread particles (GDB) and finely milled bread particles (FB).

dissolution temperature may be necessary to improve the dissolution of starch, particularly in stale bread samples, where the starch has undergone retrogradation and is surrounded or potentially entrapped by gluten and plant cell walls, which together hinder its dissolution.

CLSM was employed to observe the spatial distribution of the different components (mainly starch and protein) within the three-dimensional matrix of cryogels, xerogels and aerogels. Since it does not depend on the drying mode, CLSM images of only aerogels are shown in Fig. 5 (for xerogels and cryogels CLSM images can be found in Fig. S3). Aerogels made from samples rich in protein (i.e., Flour, Bread, and FB) displayed pixels of high red intensity indicative of the presence of protein. Compared to Flour and Bread, FB resulted in aerogels with a more uniform distribution of the protein fraction and without the presence of large protein aggregates. This result suggests that a reduction of bread particle size might homogenise the distribution of water-insoluble protein particles in the starch network. Aerogels made from

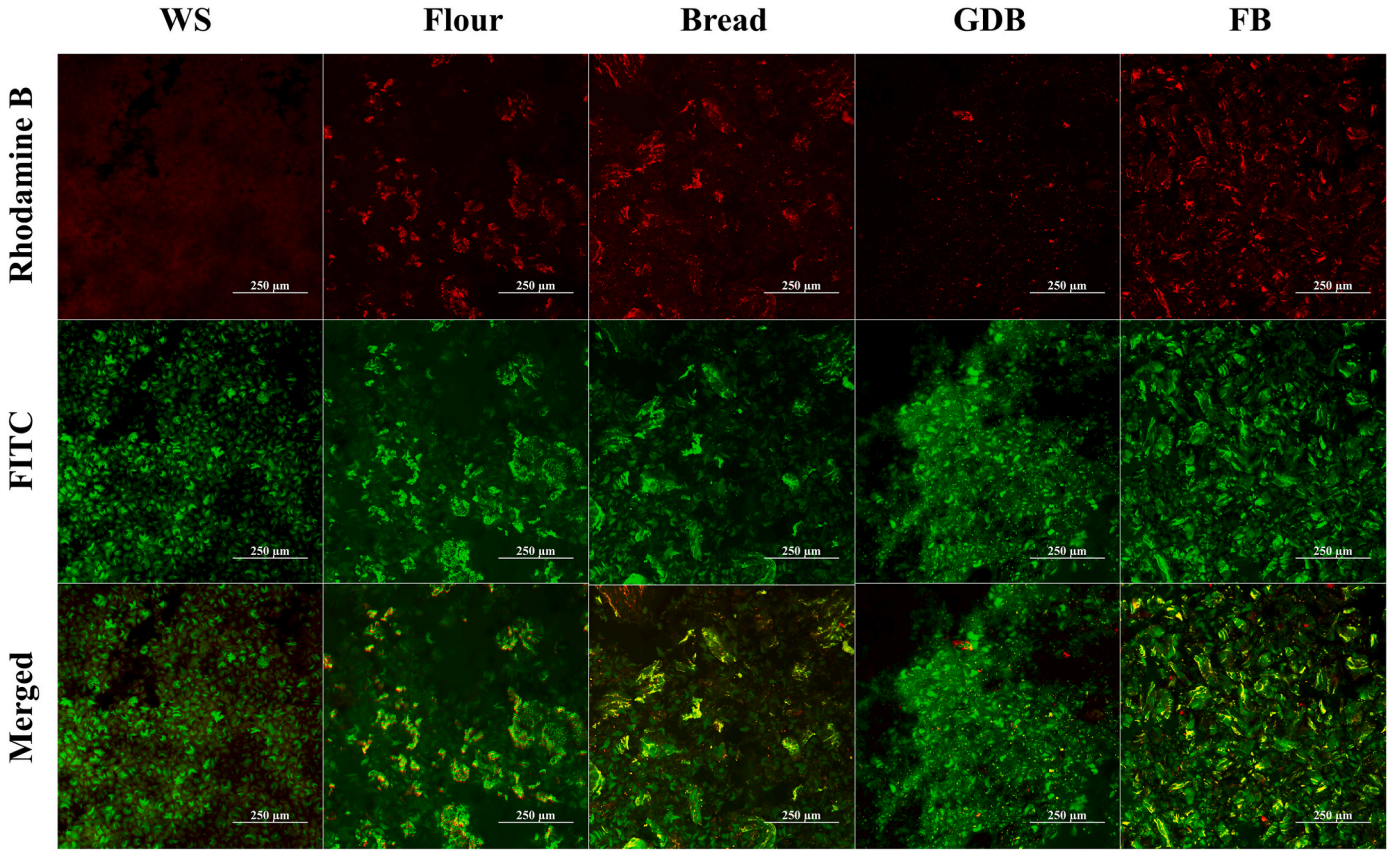

Fig. 5. CLSM images (scale bar of 250 μm) of aerogels made from wheat starch (WS), wheat flour (Flour), bread particles (Bread), gluten-depleted bread particles (GDB) and finely milled bread particles (FB). Rhodamine B was used to stain protein, whereas FITC was used to stain both starch and protein, resulting in orange and green color representing protein and starch in merged view, respectively.

samples with lower protein content (i.e., WS and GDB) displayed pixels of low red intensity, as expected. The spatial distribution of starch is indicated by the green color in the merged images. No intact granular starch was observed in any sample, which is a logical consequence from the fabrication of porous material, and further from the bread-making process in Bread, FB and GDB samples. As expected, starch clearly represented the primary component of the porous matrixes, with proteins randomly dispersed within it.

Overall, SEM and CLSM imaging suggest that the porous matrix of cryogels, xerogels and aerogels are mainly constituted by the starch network with protein, when present, dispersed throughout the matrix. In addition, the similar microstructure of xerogels and aerogels indicates that low vacuum drying could be a viable alternative to $scCO_2$ drying for fabricating finely porous materials, paving the way for novel packaging applications. Compared to xerogels and aerogels, cryogels were very brittle, easily fractured during handling, and mostly resulted in unsuitable materials for comparison purposes. Therefore, cryogels were excluded from further analysis.

3.3. X-ray diffraction

The supramolecular organization of starch in the raw materials and porous materials was investigated by X-ray diffraction. Native wheat flour presented the typical A-type crystalline pattern of cereal starches (Fig. 6A), featured by peaks of high intensity at 15.2, 17.2, 18.1 and 23.1°, and peaks of low intensity at 20.0 and 26.7° (Primo-Martín et al., 2007). This pattern is indicative of parallel, double helices separated by interstitial water. After bread-making and long-term storage, Bread particles displayed less marked peaks attributed to the starch gelatinization occurring during baking (Martínez et al., 2018). Yet, peaks at 15.2, 17.2 and 20.0° were observed, indicative of B-type crystals from retrograded starch. Compared to A-type crystals of native wheat starch, B-type crystals have more water molecules in their structure – precisely a column of water molecules replacing one of the double helices (García-González et al., 2012; Gauthier et al., 2004; Gray & Bemiller, 2003). It is noted that when water is incorporated into the B-type amylopectin crystals, it becomes structurally immobilized and is thus rendered unfreezable (Slade & Levine, 1991). It was found that crystallinity of both xerogels (Fig. S4) and aerogels (Fig. 6B) decreased compared to the initial Bread particles, suggesting the transformation of the crystalline structure into an amorphous state after dissolution and retrogradation (Zou & Budtova, 2021b). Aerogels yet showed weak peaks at 13.0, 17.2 and 20.0°, similar to previously reported wheat starch aerogels (Ubeyitogullari & Ciftci, 2016). The XRD patterns of various xerogels are shown in Fig. S4: the spectra are similar to those of aerogels, implying that the different drying approaches had no influence on starch crystallinity, likely due to the amorphous character of these materials.

3.4. Volume shrinkage, bulk density, and porosity of aerogels and xerogels

For the fabrication of both xerogels and aerogels, water molecules were eliminated from the hydrogels by solvent exchange with ethanol, resulting in alcogels that were then subjected to drying (Fig. 1). This procedure commonly induces volume shrinkage, leading to a contraction of the resultant products (Alavi & Ciftci, 2022; Zou & Budtova, 2021b, 2023). The volume shrinkage (VS) attributed to the different steps of fabrication, including solvent exchange (SE-VS), drying (D-VS), and during the whole fabrication process (F-VS), are shown in Table 2. In general, F-VS of xerogels and aerogels was very similar, within 70–80%. From a fabrication standpoint, the volume shrinkage mainly originated during solvent exchange, with values of SE-VS ranging from 62 to 78% and, hence, accounting for 87–95% of the overall fabricating shrinkage (SE-VS/F-VS) for xerogels and 91–95% for aerogels. Volume shrinkage due to the drying process (D-VS) was only around 4–11% for xerogels and 4–7% for aerogels, which can be considered negligible.

The results show that solvent exchange is the main step responsible for volume shrinkage. However, solvent exchange is necessary to produce both aerogels and xerogels. In aerogel fabrication, solvent exchange is employed to eliminate water by ethanol from the open-cell pores as water is not miscible with CO_2, the latter used to perform drying in supercritical conditions. In the fabrication of xerogels, solvent exchange with ethanol minimizes the interfacial tension between the liquid in the pores and the vapours, reducing the capillary pressure that the solid skeleton undergoes during low-vacuum evaporative drying (Zheng et al., 2020). Therefore, the decrease of SE-VS would eventually lead to a considerably lower total shrinkage, and thus increase the porosity of the resultant materials. In this regard, the different stale bread materials resulted in different SE-VS (Table 2). Bread and FB hydrogels displayed similar shrinkage upon immersion in ethanol, indicating no effect of particle size. Despite having the same amylose ratio (Table 1), SE-VS of Bread samples were higher than that of GDB samples, indicating the negative influence of protein. GDB and WS hydrogels showed the lowest (61.8%) and greatest shrinkage (78.2%) during solvent exchange, respectively. The fact that GDB and WS exhibit these differences despite having relatively similar starch purity suggests the important influence of starch features such as amylose ratio. For

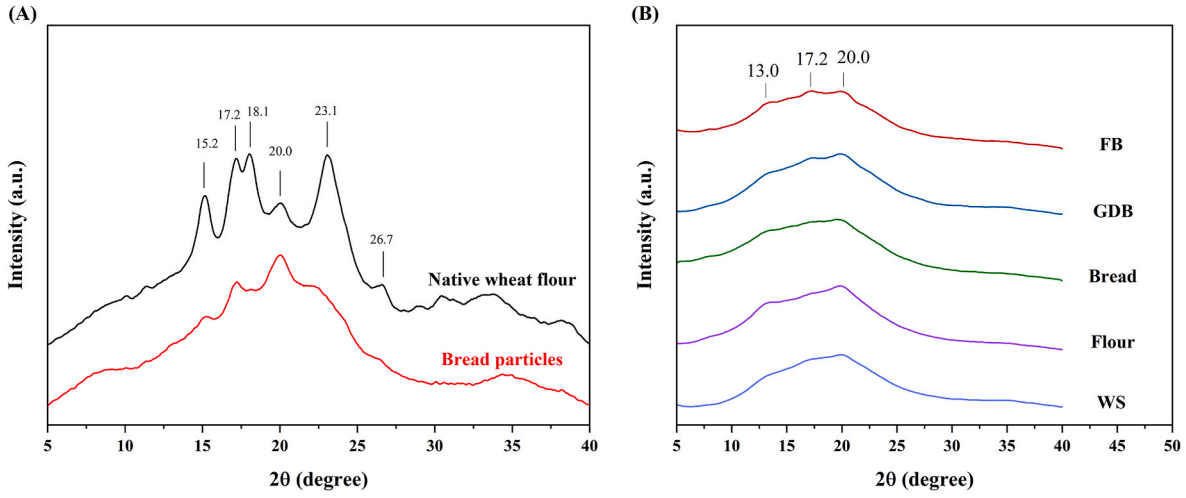

Fig. 6. X-ray diffraction pattern of native wheat flour and bread milled particles (A) and aerogels (B) made from wheat starch (WS), wheat flour (Flour), bread particles (Bread), gluten-depleted bread particles (GDB) and finely milled bread particles (FB).

Table 2
Volume shrinkage during solvent exchange (SE-VS) and drying (D-VS), total shrinkage during fabrication (F-VS), and ratio of SE-VS to F-VS for xerogels and aerogels made from wheat starch (WS), wheat flour (Flour), bread particles (Bread), gluten-depleted bread particles (GDB) and finely milled bread particles (FB).

	SE-VS (%)	D-VS (%)		SE-VS/F-VS (%)		F-VS (%)	
		Xerogel	Aerogel	Xerogel	Aerogel	Xerogel	Aerogel
WS	78.2 ± 0.4^{a}	4.3 ± 0.1^{c}	3.7 ± 0.4^{b}	95.0 ± 0.3^{a}	95.3 ± 0.2^{a}	82.3 ± 0.3^{a}	82.1 ± 0.2^{a}
Flour	75.1 ± 0.7^{b}	5.1 ± 0.4^{c}	4.5 ± 0.5^{b}	93.7 ± 0.7^{b}	94.3 ± 0.4^{a}	80.1 ± 0.6^{b}	79.6 ± 0.4^{b}
Bread	70.0 ± 1.0^{c}	8.1 ± 0.3^{b}	6.5 ± 0.7^{a}	89.2 ± 0.4^{c}	92.0 ± 1.4^{bc}	78.5 ± 0.3^{c}	76.1 ± 1.1^{c}
GDB	61.8 ± 1.0^{d}	8.3 ± 1.1^{b}	6.5 ± 0.7^{a}	87.6 ± 0.9^{d}	90.8 ± 0.7^{c}	70.5 ± 0.7^{d}	68.0 ± 0.5^{d}
FB	70.9 ± 0.7^{c}	10.9 ± 0.3^{a}	5.5 ± 0.2^{ab}	87.0 ± 0.7^{d}	92.5 ± 0.3^{b}	81.5 ± 0.6^{a}	76.7 ± 0.3^{c}

Letters represent significant difference within the same column ($p < 0.05$).

example, it was demonstrated that retrograded pea starch hydrogels (33–36% amylose) are stronger than retrograded potato starch hydrogels (18–21% amylose), the former better resisting solvent/non-solvent exchange (Zou & Budtova, 2021b). Besides, the SE-VS of alcogels prepared from Bread, FB and GDB, which were all featured by a higher amylose ratio, was found lower than SE-VS of WS and Flour alcogels, again suggesting a positive effect of higher amylose ratio. These results might support the findings on starch-based porous materials showing that a reduction of volumetric shrinkage of aerogels can be achieved with higher amylose ratio (Alavi & Ciftci, 2023; Druel et al., 2017; Zou & Budtova, 2021b). Simultaneously, these bread samples also presented amylopectin and amylose of lower molar mass than WS and Flour. Further experiments are needed to pinpoint the influence of amylopectin and amylose molecular weight or a combination of both.

Influenced by fabrication shrinkage, samples exhibited the corresponding differences in density and porosity, where porosity was inversely aligned with density (Table 3). No significant differences in porosity and density between xerogels and aerogels were observed, confirming morphology observations (Fig. 4). Among samples, particle size generally had no effect on the porous properties. GDB samples presented the lowest density (0.26 g/cm^3 for xerogel and 0.22 g/cm^3 for aerogel) and greatest porosity (82.9% for xerogel and 85.3% for aerogel), whereas WS samples presented the highest density and lowest porosity, most probably because differences in amylose ratio and starch molecular features. Overall, our porous starches possess densities within the interval of those of other starch aerogels made from 10 wt% solutions reported in literature: from 0.11 g/cm^3 for wheat starch (Ubeyitogullari et al., 2019) to 0.2 g/cm^3 for corn starch (Santos-Rosales et al., 2020) and 0.4–0.5 g/cm^3 for potato starch (Zou & Budtova, 2021b). It should be noted that starch aerogel properties also strongly depend on retrogradation time, making challenging an adequate comparison with literature data.

Based on the results presented above, stale bread with higher amylose ratio results in materials of greater porosity and lower density compared to commercial wheat starch, denoting the potential of stale bread to be directly upcycled into porous materials by simple solvent exchange and low-vacuum drying. Furthermore, the removal of gluten from stale bread could enhance the porous properties of resultant materials.

Table 3
Density, porosity, and specific surface area (S_{BET}) of xerogels and aerogels made from wheat starch (WS), wheat flour (Flour), bread particles (Bread), gluten-depleted bread particles (GDB) and finely milled bread particles (FB).

	Density (g/cm^3)		Porosity (%)		Specific surface area (m^2/g)	
	Xerogel	Aerogel	Xerogel	Aerogel	Xerogel	Aerogel
WS	0.47 ± 0.02^{a}	0.46 ± 0.01^{a}	68.4 ± 1.1^{c}	69.1 ± 0.4^{e}	36 ± 1^{c}	36 ± 0^{d}
Flour	0.34 ± 0.01^{b}	0.35 ± 0.00^{b}	77.1 ± 0.8^{b}	76.4 ± 0.1^{d}	38 ± 0^{c}	41 ± 1^{c}
Bread	0.33 ± 0.00^{b}	0.28 ± 0.01^{d}	78.0 ± 0.2^{b}	81.3 ± 0.7^{b}	38 ± 1^{c}	40 ± 1^{c}
GDB	0.26 ± 0.01^{c}	0.22 ± 0.01^{e}	82.9 ± 0.9^{a}	85.3 ± 0.4^{a}	72 ± 0^{a}	79 ± 0^{a}
FB	0.33 ± 0.02^{b}	0.32 ± 0.00^{c}	77.8 ± 1.2^{b}	78.6 ± 0.3^{c}	60 ± 1^{b}	61 ± 0^{b}

Letters indicate significant difference within the same column ($p < 0.05$).

3.5. Specific surface area

Porous materials generally displayed a higher specific surface area than dense materials, providing a unique opportunity of bioactive compounds incorporation. Specific surface area (S_{BET}) values of aerogels and xerogels are shown in Table 3, varying from 36 to 72 m^2/g for xerogels and from 36 to 79 m^2/g for aerogels, which is similar to some potato and wheat starch aerogels (Ubeyitogullari and Ciftci, 2016)) but lower than that of pea starch aerogels (Zou and Budtova, 2021b). As well as for other material characteristics, a comparison with the results from literature is challenging as specific surface area depends on numerous parameters such as starch type and purity, concentration in solution, retrogradation time, type of non-solvent and drying conditions (for example, temperature, pressure and depressurisation rate during supercritical drying). No differences between xerogels and aerogels S_{BET} was found within the experimental errors (< 10%), indicating that indeed it was possible to produce aerogel-like materials using low vacuum drying.

Among our samples, Bread, Flour, and WS porous materials exhibited a similar S_{BET} value of 36–39 m^2/g for xerogels and 36–42 m^2/g for aerogels, which was lower than the S_{BET} of GDB and FB. Flour and Bread are rich in protein, and WS has the lowest amylose ratio. It is hypothesized that gluten inhibits the formation of the fine pores in starch network, leading to a lower S_{BET}. Larger pores in cryogels based on starches with higher protein content confirm this assumption (Fig. S2). The composition of the starting matter is thus the reason of different specific surface area among samples prepared with the same conditions. For example, it was demonstrated that higher amylose ratio leads to higher surface area (Druel et al., 2017; Zou & Budtova, 2021b). At any event, our results showed that porous materials with certain mesoporosity (surface area 60–80 m^2/g) can be attained using stale bread as starting matter (Table 3). Importantly, GDB porous materials exhibited a two-fold higher S_{BET} than that of WS, Flour, and Bread, reaching similar and even higher values than for aerogels (48–62 m^2/g) made from 10 wt % wheat starch (25% amylose) (Ubeyitogullari & Ciftci, 2016; Ubeyitogullari et al., 2018). This might suggest the combined influence of amylose ratio and starch molecular characteristics on a 'finesse' of starch network.

3.6. Water absorption capacity and mechanical properties

Considering the porous structure of the materials obtained, their water absorption capacity (WAC) and mechanical properties were determined (Table 4) in the view of their potential utilization as absorbent pads, or for packaging applications such as loose-fill cushioning materials. After 24 h soaking in water, Bread, FB, Flour, and WS materials possessed similar WAC for both xerogels and aerogels, with percentage difference between xerogels and aerogels of the same

Table 4
Water absorption capacity and mechanical properties of xerogels and aerogels made from wheat starch (WS), wheat flour (Flour), bread particles (Bread), gluten-depleted bread particles (GDB) and finely milled bread particles (FB).

	Water absorption capacity (%)		Maximum compressive stress (kPa)		Compressive modulus (MPa)		Strain at failure (%)	
	Xerogel	Aerogel	Xerogel	Aerogel	Xerogel	Aerogel	Xerogel	Aerogel
WS	319 ± 7^{c}	354 ± 15^{b}	2241.9 ± 67.5^{a}	1987.7 ± 102.4^{a}	9.9 ± 2.6^{a}	5.7 ± 1.4^{a}	33.3 ± 3.9^{a}	35.2 ± 2.2^{b}
Flour	392 ± 37^{b}	395 ± 31^{b}	424.1 ± 49.1^{b}	519.2 ± 49.2^{b}	4.1 ± 0.32^{b}	4.4 ± 0.8^{a}	25.0 ± 1.4^{b}	28.0 ± 2.4^{c}
Bread	376 ± 13^{bc}	404 ± 10^{b}	186.3 ± 10.6^{c}	144.1 ± 19.1^{c}	2.4 ± 0.2^{b}	1.5 ± 0.2^{b}	18.3 ± 0.9^{c}	18.5 ± 3.9^{d}
GDB	486 ± 20^{a}	599 ± 23^{a}	475.1 ± 48.4^{b}	590.2 ± 67.2^{b}	3.2 ± 0.5^{b}	2.4 ± 0.3^{b}	36.9 ± 1.8^{a}	41.6 ± 3.8^{a}
FB	351 ± 22^{bc}	395 ± 28^{b}	235.2 ± 20.5^{c}	184.3 ± 17.1^{c}	3.8 ± 0.4^{b}	1.2 ± 0.1^{b}	15.7 ± 1.8^{c}	25.4 ± 1.8^{c}

Letters represent significant difference within the same column ($p < 0.05$).

formulation below 12% and WAC values ranging from around 320 to 390 % for xerogels and 350–400 % for aerogels. Bread and FB samples were partly losing their integrity in water while WS and GDB samples kept their uniform network. GDB materials presented the greatest WAC, with noticeable difference between xerogel (~490%) and aerogel (~600%), whereas WS materials showed the lowest WAC among all samples. These results are aligned with density and porosity trends, where a higher porosity and lower density led to a higher absorption of water (Fig. 7A). Except for GDB materials, WAC values were lower than those of cryogels reported in other studies: for example, cryogels from native corn starch were reported to present WAC from 540 to 730 % (Fonseca et al., 2021); from germinated wheat starch with porosity of 89% from 580 to 1000 % (Silva et al., 2023); and from native potato starch around 1100% (Kaster et al., 2024). The difference in WAC between those studies and the samples from the current study could be explained by many factors, such as starch concentration, fabrication approach, and differences in starch features as affected by different plant species and cultivars. In any case, GDB materials still presented comparative WAC to corn starch cryogels (Fonseca et al., 2021), suggesting a plausible potential of using GDB porous materials as absorbent pad.

Even though cryogels from other studies exhibited greater WAC than our developed porous materials, it is noteworthy that cryogels are usually fragile, which results in poor handling, as observed in the present work. To evaluate the mechanical properties of our aerogels and xerogels, uniaxial compression was performed. The stress-strain dependences are presented in Fig. 7B. The maximum compressive stress (at break), compressive modulus and strain at failure are listed in Table 4, and compressive modulus and stress as a function of material density are shown in Fig. 7C and D, respectively. Unlike different bio-aerogels which were densified under compression and do not break (Buchtova et al., 2019; Chen et al., 2022), our porous materials presented a brittle

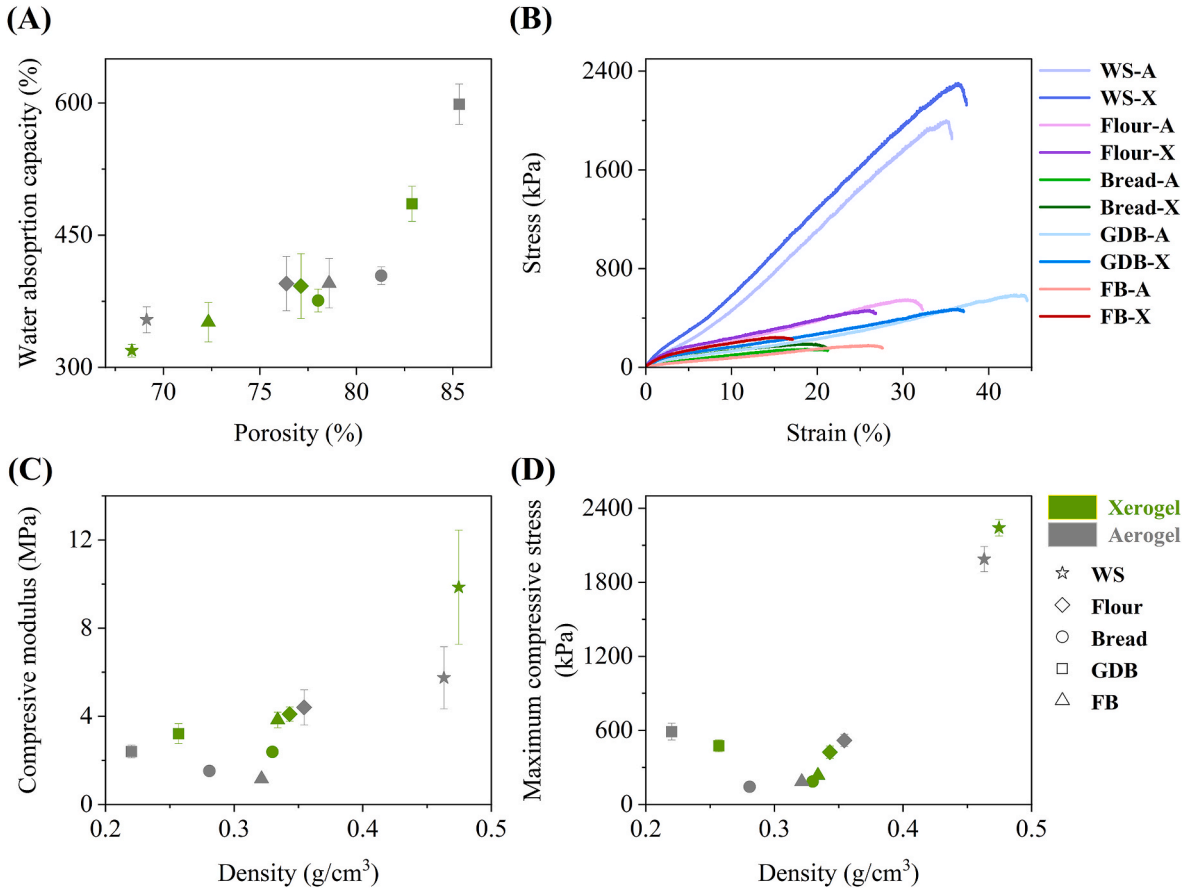

Fig. 7. Relationship between water absorption capacity and porosity in xerogels and aerogels (A). Stress-strain curve of xerogels (-X) and aerogels (-A) made from wheat starch (WS), wheat flour (Flour), bread particles (Bread), gluten-depleted bread particles (GDB) and finely milled bread particles (FB). Curves of a lighter color represent aerogels, while those of a darker color of the same hue represent xerogels. Relationship between density and compressive modulus (C) and maximum compressive stress (D) in xerogels and aerogels.

behaviour at high compressive stresses (Fig. 7B). Practically no differences in the mechanical properties of aerogels and xerogels of the same density was observed, as depicted in Fig. 7C and D. As expected, compressive stress and modulus increase with density increase, with a deviation for Bread and FB, the latter presumably due to the spatial interference of protein leading to a less interconnected starch network. The negative effect of water insoluble gluten was further evidenced by the fact that the compressive stress was improved after gluten depletion. Despite displaying differences in starch structure and amylose ratio (Table 1), GDB materials displayed compressive stress similar to Flour materials, presumably indicating an effect of starch structural features. A similar hypothesis was made by Wang et al. (2018), who stated that amylopectin with higher branch density induces greater rigidity of the starch structure than the linear polymers. This mechanism could be inferred from WS materials as well, which exhibited the greatest compressive stress (2.2 MPa for xerogel and 2.0 MPa for aerogel), being significantly higher than the rest of the porous materials and aligning to its starch molecular characteristics (Table 1).

Coherent with compressive stress, WS materials presented the greatest compressive modulus (9.9 MPa for xerogel and 5.8 MPa for aerogel) among samples (Table 3), which may be due to material higher density (Fig. 7C). It is noted that although Flour, Bread, FB and GDB porous materials showed lower compressive modulus (2.4–4.1 MPa for xerogels and 1.2–4.4 MPa for aerogels) than WS materials in this work, they were still significantly higher than cryogels prepared from pulse starches (Falua et al., 2023). Density of pulse starch cryogel was below 0.12 g/cm^3, significantly lower than those of bread-based materials (> 0.26 g/cm^3). Therefore, the higher mechanical stress and modulus was mainly ascribed to the higher densities of our materials (Fig. 7C and D). These results thus highlight the stronger structure and mechanical performance of our porous materials based on stale bread.

All our porous materials displayed strain at failure with values of xerogels and aerogels ranging from 18 to 37 % and from 19 to 42 %, respectively. No significant differences between Bread and FB were observed, suggesting that initial particle size played a minor role on the mechanical properties. WS materials exhibited higher strain at failure (33.3% for xerogels and 35.3% for aerogels) than the other samples except for GDB materials, which could be attributed to the combination of large starch molecules and high starch purity that presumably led to a strong and uniform starch matrix (Table 1) resilient to the compressive force. Remarkably, GDB presented the greatest strain at failure for both xerogels (36.9%) and aerogels (41.6%), indicating the importance of gluten removal and suggesting an important contribution of both starch purity, starch structural features and high porosity to attaining a homogeneous, flexible, and porous matrix.

4. Conclusions

In this work, 100% bio-based, low-density materials with partial mesoporosity were made from stale white bread, an abundant and unpolluted waste stream with gelatinized starch as its main constituent. Gluten-depleted bread, finely milled bread, and also wheat starch and wheat flour were used to investigate the influence of the presence of protein, particle size and starch molecular features such as amylose ratio on materials' properties. The starting materials were gelatinized followed by different processing pathways: freeze-drying of hydrogels resulting in cryogels, and water exchange to ethanol to make xerogels via evaporative drying in low vacuum or to make aerogels via drying with supercritical CO_2. Cryogels were highly porous but very brittle thus difficult to handle. Xerogels and aerogels turned out to possess very similar morphology and properties opening the way of making lightweight materials with certain mesoporosity avoiding high-pressure technology, thus significantly reducing process costs.

Overall, xerogels and aerogels from stale bread exhibited similar or even superior performance to those from commercial pure starch in terms of volume shrinkage, density, and porosity. This supports our hypothesis that bread waste can be directly exploited as a polymeric building block for future (meso)porous materials for packaging applications. Remarkably, depleting gluten from stale bread particles through enzymatic proteolysis resulted in xerogels and aerogels with the lowest volume shrinkage and density, and the greatest porosity, specific surface area, water absorption capacity, and strain at failure among all materials, including those made from commercial wheat starch. In some instances, reducing the particle size of stale bread particles enhanced the porous properties of the resulting materials (e.g., by increasing the specific surface area), although this effect was much more moderate than the effect of gluten depletion. Simple gluten depletion through enzymatic proteolysis or particle size reduction can thus tune the properties of bread waste (meso)porous materials to adjust them to various applications.

Bio-based mesoporous materials offer several environmentally friendly applications due to their renewable and biodegradable nature, and in the case of those from stale bread, benefiting from the upcycling of a waste stream. In catalysis and pollutant adsorption, bread-based porous materials could provide a green alternative to traditional synthetic materials, supporting sustainable environmental remediation. They might also be attractive as matrices delivering fertilizers for agriculture, or for biodegradable packaging in the food and pharmaceutical industries, offering eco-friendly alternatives to plastic. This includes potential applications as loose-fill cushioning material, replacing polystyrene, as well as absorbent pads in food packaging due to their high absorptive capacity. Additionally, when encapsulated with bioactive compounds, they could serve as bioactive packaging with a larger surface area than polystyrene. Furthermore, in energy storage or construction materials, bio-based mesoporous materials could advance the development of greener technologies with reduced environmental impact. This study is anticipated to set a precedent for future research on combining stale bread with other polymers to replicate the performance of non-biodegradable porous materials for numerous applications.

CRediT authorship contribution statement

Wanxiang Guo: Writing – original draft, Methodology, Investigation, Conceptualization. **Tatiana Budtova:** Writing – review & editing, Visualization, Supervision. **Mario M. Martinez:** Writing – review & editing, Visualization, Supervision, Funding acquisition, Conceptualization.

Declaration of competing interest

The authors declare that they have no known competing financial interests or personal relationships that could have appeared to influence the work reported in this paper.

Acknowledgments

This research was funded by Independent Research Fund Denmark - Danmarks Frie Forskningsfond (project number 1032-00491B). The authors also acknowledge the financial support from China Scholarship Council (CSC), William Demant Fonden, Otto Mønsted Foundation, and Fællesfonden. Some of the data was generated through accessing research infrastructure funded by FOODHAY (Food and Health Open Innovation Laboratory, Danish Roadmap for Research Infrastructure). The authors also acknowledge La Tahona de Sahagun and Maria Franco for providing the industrial environment to obtain the wheat flours and breads. The authors would also like to thank Julia Spotti from Aarhus University, and Hiba Bouras, Sujie Yu and Lionel Freire (all from CEMEF, Mines Paris) for their experimental support and Julien Jaxel (PERSEE, Mines Paris) for supercritical drying.

Appendix A. Supplementary data

Supplementary data to this article can be found online at https://doi.org/10.1016/j.foodhyd.2024.110807.

Data availability

Data will be made available on request.

References

AACC. (2010). *Approved methods of the American* (11 ed.). St. Paul: American Association of Cereal Chemists https://www.cerealsgrains.org/resources/Methods/Pages/default.aspx.

Ahmadzadeh, S., & Ubeyitogullari, A. (2023). Generation of porous starch beads via a 3D food printer: The effects of amylose content and drying technique. *Carbohydrate Polymers, 301*(Pt A), Article 120296. https://doi.org/10.1016/j.carbpol.2022.120296

Alavi, F., & Ciftci, O. N. (2022). Developing dual nano/macroporous starch bioaerogels via emulsion templating and supercritical carbon dioxide drying. *Carbohydrate Polymers, 292*, Article 119607. https://doi.org/10.1016/j.carbpol.2022.119607

Alavi, F., & Ciftci, O. N. (2023). Effect of starch type and chitosan supplementation on physicochemical properties, morphology, and oil structuring capacity of composite starch bioaerogels. *Food Hydrocolloids, 141*, Article 108637. https://doi.org/10.1016/j.foodhyd.2023.108637

Barros, J. H. T., Frasson, S. F., & Colussi, R. (2024). Characterization of pupunha starch (*Bactris gasipaes* var. gasipaes) and its application in aerogel production. *Food Bioscience, 59*, Article 104243. https://doi.org/10.1016/j.fbio.2024.104243

Brancoli, P., Bolton, K., & Eriksson, M. (2020). Environmental impacts of waste management and valorisation pathways for surplus bread in Sweden. *Waste Management, 117*, 136–145. https://doi.org/10.1016/j.wasman.2020.07.043

Brancoli, P., Lundin, M., Bolton, K., & Eriksson, M. (2019). Bread loss rates at the supplier-retailer interface – analysis of risk factors to support waste prevention measures. *Resources, Conservation and Recycling, 147*, 128–136. https://doi.org/10.1016/j.resconrec.2019.04.027

Brancoli, P., Rousta, K., & Bolton, K. (2017). Life cycle assessment of supermarket food waste. *Resources, Conservation and Recycling, 118*, 39–46. https://doi.org/10.1016/j.resconrec.2016.11.024

Buchtova, N., Pradille, C., Bouvard, J. L., & Budtova, T. (2019). Mechanical properties of cellulose aerogels and cryogels. *Soft Matter, 15*(39), 7901–7908. https://doi.org/10.1039/c9sm01028a

Campanella, J. M. B. O. H. (2014). *Extrusion processing technology: Food and non-food biomaterials* (1st ed.). John Wiley & Sons, Ltd.

Chen, L., Niu, X., Fan, X., Liu, Y., Yang, J., Xu, X., Zhou, G., Zhu, B., Ullah, N., & Feng, X. (2022). Highly absorbent antibacterial chitosan-based aerogels for shelf-life extension of fresh pork. *Food Control, 136*, Article 108644. https://doi.org/10.1016/j.foodcont.2021.108644

Dengate, H. N., Baruch, D. W., & Meredith, P. (1978). The density of wheat starch granules: A tracer dilution procedure for determining the density of an immiscible dispersed phase. *Starch - Stärke, 30*(3), 80–84. https://doi.org/10.1002/star.19780300304

Druel, L., Bardl, R., Vorwerg, W., & Budtova, T. (2017). Starch aerogels: A member of the family of thermal superinsulating materials. *Biomacromolecules, 18*(12), 4232–4239. https://doi.org/10.1021/acs.biomac.7b01272

Dymchenko, A., Geršl, M., & Gregor, T. (2023). Trends in bread waste utilisation. *Trends in Food Science & Technology, 132*, 93–102. https://doi.org/10.1016/j.tifs.2023.01.004

Eriksson, M., Strid, I., & Hansson, P.-A. (2015). Carbon footprint of food waste management options in the waste hierarchy – a Swedish case study. *Journal of Cleaner Production, 93*, 115–125. https://doi.org/10.1016/j.jclepro.2015.01.026

Falua, K. J., Babaei-Ghazvini, A., & Acharya, B. (2023). Comparative study of the structure and mechanical properties of starch aerogels fabricated from air-classified and isolated pulse starches. *International Journal of Biological Macromolecules, 257*(Pt 1), Article 128478. https://doi.org/10.1016/j.ijbiomac.2023.128478

Fonseca, L. M., Silva, F. T. D., Bruni, G. P., Borges, C. D., Zavareze, E. D. R., & Dias, A. R. G. (2021). Aerogels based on corn starch as carriers for pinhao coat extract (Araucaria angustifolia) rich in phenolic compounds for active packaging. *International Journal of Biological Macromolecules, 169*, 362–370. https://doi.org/10.1016/j.ijbiomac.2020.12.110

Franco, M., Spotti, M. J., Gomez, M., & Martinez, M. M. (2024). Understanding the influence of the arabinoxylan-rich psyllium (Plantago ovata) husk on dough elasticity and bread staling: Interplay between biopolymer and water dynamics. *Food Hydrocolloids, 154*, Article 110099. https://doi.org/10.1016/j.foodhyd.2024.110099

García-González, C. A., Camino-Rey, M. C., Alnaief, M., Zetzl, C., & Smirnova, I. (2012). Supercritical drying of aerogels using CO_2: Effect of extraction time on the end material textural properties. *The Journal of Supercritical Fluids, 66*, 297–306. https://doi.org/10.1016/j.supflu.2012.02.026

Gauthier, B. M., Bakrania, S. D., Anderson, A. M., & Carroll, M. K. (2004). A fast supercritical extraction technique for aerogel fabrication. *Journal of Non-crystalline Solids, 350*, 238–243. https://doi.org/10.1016/j.jnoncrysol.2004.06.044

Gómez, M., & Martinez, M. M. (2023). Redistribution of surplus bread particles into the food supply chain. *LWT-Food Science & Technology, 173*, Article 114281. https://doi.org/10.1016/j.lwt.2022.114281

Gray, J. A., & Bemiller, J. N. (2003). Bread staling: Molecular basis and control. *Comprehensive Reviews in Food Science and Food Safety, 2*(1), 1–21. https://doi.org/10.1111/j.1541-4337.2003.tb00011.x

Gruppen, H., Marseille, J. P., Voragen, A. G. J., Hamer, R. J., & Pilnik, W. (1989). Mild isolation of water-insoluble cell wall material from wheat flour: Composition of fractions obtained with emphasis on non-starch polysaccharides. *Journal of Cereal Science, 9*(3), 247–260. https://doi.org/10.1016/S0733-5210(89)80007-4

Guo, W., Spotti, M. J., Portillo-Perez, G., Bonilla, J. C., Bai, W., & Martinez, M. M. (2024). Molecular changes and interactions of wheat flour biopolymers during bread-making: Implications to upcycle bread waste into bioplastics. *Carbohydrate Polymers, 342*, Article 122414. https://doi.org/10.1016/j.carbpol.2024.122414

Kaster, J. B., Cruz, E. P. D., Silva, F. T. D., Hackbart, H., Siebeneichler, T. J., Camargo, T. M., Radunz, M., Fonseca, L. M., & Zavareze, E. D. R. (2024). Bioactive aerogels based on native and phosphorylated potato (Solanum tuberosum L.) starches incorporated with star fruit extract (Averrhoa carambola L.). *International Journal of Biological Macromolecules, 272*(Pt 2), Article 132907. https://doi.org/10.1016/j.ijbiomac.2024.132907

Kumar, V., Brancoli, P., Narisetty, V., Wallace, S., Charalampopoulos, D., Kumar Dubey, B., Kumar, G., Bhatnagar, A., Kant Bhatia, S., & Taherzadeh, M. J. (2022). Bread waste – a potential feedstock for sustainable circular biorefineries. *Bioresource Technology, 269*, Article 128449. https://doi.org/10.1016/j.biortech.2022.128449

Ma, B., Hou, X. B., & Li, Y. (2022). Mechanically strong and thermal insulating polyimide/SiO_2 aerogel prepared by ambient drying. *Materials Letters, 327*, Article 133039. https://doi.org/10.1016/j.matlet.2022.133039

Martínez, M. M., Román, L., & Gómez, M. (2018). Implications of hydration depletion in the in vitro starch digestibility of white bread crumb and crust. *Food Chemistry, 239*, 295–303. https://doi.org/10.1016/j.foodchem.2017.06.122

Narisetty, V., Cox, R., Willoughby, N., Aktas, E., Tiwari, B., Matharu, A. S., Salonitis, K., & Kumar, V. (2021). Recycling bread waste into chemical building blocks using a circular biorefining approach. *Sustainable Energy Fuels, 5*(19), 4842–4849. https://doi.org/10.1039/d1se00575h

Primo-Martín, C., van Nieuwenhuijzen, N. H., Hamer, R. J., & van Vliet, T. (2007). Crystallinity changes in wheat starch during the bread-making process: Starch crystallinity in the bread crust. *Journal of Cereal Science, 45*(2), 219–226. https://doi.org/10.1016/j.jcs.2006.08.009

Roman, L., Gomez, M., Li, C., Hamaker, B. R., & Martinez, M. M. (2017). Biophysical features of cereal endosperm that decrease starch digestibility. *Carbohydrate Polymers, 165*, 180–188. https://doi.org/10.1016/j.carbpol.2017.02.055

Santos-Rosales, V., Alvarez-Rivera, G., Hillgärtner, M., Cifuentes, A., Itskov, M., García-González, C. A., & Rege, A. (2020). Stability studies of starch aerogel formulations for biomedical applications. *Biomacromolecules, 21*(12), 5336–5344. https://doi.org/10.1021/acs.biomac.0c01414

Silva, F. T., Fonseca, L. M., Bruni, G. P., Crizel, R. L., Oliveira, E. G., Zavareze, E. D., & Dias, A. R. G. (2023). Absorbent bioactive aerogels based on germinated wheat starch and grape skin extract. *International Journal of Biological Macromolecules, 249*, Article 126108. https://doi.org/10.1016/j.ijbiomac.2023.126108

Slade, L., & Levine, H. (1991). Beyond water activity: Recent advances based on an alternative approach to the assessment of food quality and safety. *Critical Reviews in Food Science and Nutrition, 30*(2–3), 115–360. https://doi.org/10.1080/10408399109527543

Ubeyitogullari, A., Brahma, S., Rose, D. J., & Ciftci, O. N. (2018). In vitro digestibility of nanoporous wheat starch aerogels. *Journal of Agricultural and Food Chemistry, 66*(36), 9490–9497. https://doi.org/10.1021/acs.jafc.8b03231

Ubeyitogullari, A., & Ciftci, O. N. (2016). Formation of nanoporous aerogels from wheat starch. *Carbohydrate Polymers, 147*, 125–132. https://doi.org/10.1016/j.carbpol.2016.03.086

Ubeyitogullari, A., Moreau, R., Rose, D. J., Zhang, J., & Ciftci, O. N. (2019). Enhancing the bioaccessibility of phytosterols using nanoporous corn and wheat starch bioaerogels. *European Journal of Lipid Science and Technology, 121*, Article 1700229. https://doi.org/10.1002/ejlt.201700229

Wang, S., Wang, F., Lu, C., Ma, S., Gu, Y., & Wang, L. (2024). Citral-loaded nanocellulose/sodium alginate aerogel packaging liner for fresh pork preservation. *Food Control, 155*. https://doi.org/10.1016/j.foodcont.2023.110031

Wang, Y., Wu, K., Xiao, M., Riffat, S. B., Su, Y., & Jiang, F. (2018). Thermal conductivity, structure and mechanical properties of konjac glucomannan/starch based aerogel strengthened by wheat straw. *Carbohydrate Polymers, 197*, 284–291. https://doi.org/10.1016/j.carbpol.2018.06.009

Zheng, Q., Tian, Y., Ye, F., Zhou, Y., & Zhao, G. (2020). Fabrication and application of starch-based aerogel: Technical strategies. *Trends in Food Science & Technology, 99*, 608–620. https://doi.org/10.1016/j.tifs.2020.03.038

Zhu, F. (2019). Starch based aerogels: Production, properties and applications. *Trends in Food Science & Technology, 89*, 1–10. https://doi.org/10.1016/j.tifs.2019.05.001

Zou, F., & Budtova, T. (2021a). Polysaccharide-based aerogels for thermal insulation and superinsulation: An overview. *Carbohydrate Polymers, 266*, Article 118130. https://doi.org/10.1016/j.carbpol.2021.118130

Zou, F., & Budtova, T. (2021b). Tailoring the morphology and properties of starch aerogels and cryogels via starch source and process parameter. *Carbohydrate Polymers, 255*, Article 117344. https://doi.org/10.1016/j.carbpol.2020.117344

Zou, F., & Budtova, T. (2023). Starch alcogels, aerogels, and aerogel-like xerogels: Adsorption and release of theophylline. *ACS Sustainable Chemistry & Engineering, 11*(14), 5617–5625. https://doi.org/10.1021/acssuschemeng.2c07762